Low temperature mechanism of adsorption of methane: Comparison between homogenous and heterogeneous pores

Ege Dundar[a], Justyna Rogacka[b], Lucyna Firlej[c,d], Carlos Wexler[d], Philip Llewellyn[a], Pascal Boulet[a], Bogdan Kuchta[a,d,*]

[a] Laboratoire MADIREL, Université Aix-Marseille, CNRS UMR 7246, 13396 Marseille, France
[b] Group of Bioprocess and Biomedical Engineering, Technical University of Wroclaw, Wroclaw, Poland [c] Laboratoire Charles Coulomb (L2C), UMR 5221CNRS-Université de Montpellier, Montpellier, France [d] Department of Physics and Astronomy, University of Missouri, Columbia, MO 65211, USA

abstract

The mechanisms of methane adsorption in (i) homogeneous carbon slit pores of widths between 1 nm and 2 nm and (ii) heterogeneous MOF pores of similar unit cell sizes have been compared. We discuss the mechanism of layering transition in subcritical conditions, for temperatures between 80 K and 180 K. The layer formation is strongly temperature-dependent. In slit pores it varies from a sharp adsorption at low temperatures to a more continuous uptake at higher temperatures. The pore size defines the number of adsorbed layers: the 1 nm pore allows adsorption of 2 layers while the 2 nm pore allows adsorption of 5 layers of methane molecules. We compare this behavior with the mechanism of adsorption in two MOFs, IRMOF-1 and IRMOF-16, with strongly heterogeneous walls (both structurally and energetically). This comparison allows us to discuss separately the influence of wall topology and intermolecular interactions on the mechanism of layering.

1. Introduction

In order to efficiently use adsorption-based processes in indus- trial applications it is crucial to fully understand the underlying fundamental adsorption mechanisms. Extended information about gas adsorption at ambient temperature is available in the literature [1–5]; however, it is also important, for a variety of microporous materials (like activated carbon, graphene and zeolites), to investigate the properties of low temperature adsorbed phases [6–8]. Methane adsorbed in confined geometries is interesting from both fundamental and practical points of view. At ambient temperatures supercritical adsorption is usually studied, as it is the most relevant for methane storage. At the same time, the analysis of methane's low temperature adsorption can provide a deep insight into the mechanism of adsorption as a function of industrially relevant parameters such as temperature, pore size, and pore topology.

In recent years, a new class of crystalline microporous materials has emerged: metal–organic frameworks (MOFs) [9–11]. MOFs are organic–inorganic materials showing a large spectrum of adsorption characteristics. The most remarkable is the modular approach used to synthesize them [12]. The use of independent building units (organic linkers and metal nodes) offers a large synthesis flexibility and allows tailoring specific physical characteristics and chemical functionalities of these highly porous materials [13]. MOFs belong- ing to the IRMOF family (IsoReticular metal–organic frameworks) [11], have been identified as excellent candidates for methane storage, at room temperature and for pressures up to 42 bar (in the case of IRMOF-6). Some of them show unusual adsorption of methane, in which an evolution from type V isotherms at low temperature to type I isotherms at higher temperature has been observed [12]. Grand canonical Monte Carlo (GCMC) simulations showed that this behavior results from relatively weak methane–pore wall interactions, which in turn, is a consequence of the relatively open nature of the MOF framework. The temperature at which transition from a type V isotherm to a type I isotherm occurs strongly depends on pore size, particularly for IRMOFs with smaller pores.

The properties of any adsorbed system are determined by the competition between two types of interactions: adsorbate–adsorbate and adsorbate–adsorbent. This competition defines, in particular, the shape of the isotherms and the structure of the adsorbed phase. The existence of an inflection point in the isotherm may be an indication that the adsorbate–adsorbate interaction is getting stronger than the adsorbate–absorbent one.

Capillary condensation in nanopores is another consequence of the domination of intra-adsorbate interactions. When the multilayer adsorption occurs in nanopores, the mechanism of the layer formation is also governed by this competition because the subsequent layers feel weaker attraction from the wall atoms. However, there is another important factor that influences the mechanism of adsorption: the heterogeneity of the adsorbent. The heterogeneity may modulate the energy competition and substantially modify the adsorption mechanism. For instance, the ordered monolayer is formed only in the case of a very homogeneous surface. In the case of strongly heterogeneous adsorbents the well-defined monolayers do not form and the notion of 'statistical monolayer' is used to describe the situation. In this paper we focus our analysis on the influence of pore wall heterogeneity on the mechanism of layer formation in micropores, that is, pores which can accommodate no more than five layers of methane molecules.

We present simulations of methane adsorption in two different adsorbents: graphene slit-shaped pores with homogeneous (smooth) pore walls and of effective widths between 1 and 2 nm, and two IRMOFs, IRMOF-1 and IRMOF-16 (see Fig. 1) (having pore sizes of 1.24 nm and 2.12 nm, respectively) characterized by very heterogeneous pore walls. The pore sizes are given as the distances between the wall-atom positions. Our goal is to analyze the influence of pore wall heterogeneity on the structural properties of methane adsorbed in MOFs. In particular, we compare the mechanisms of layering transition and possible occurrence of capillary condensation. Finally, we will point out that the pore filling in MOFs is an intricate process having some similarities to structural phase transition.

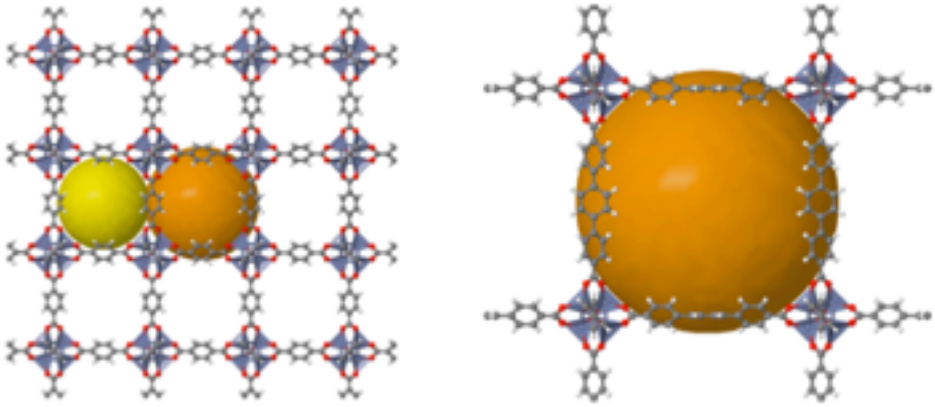

Fig. 1. Graphical representations of the IRMOFs studied in this work: (left) IRMOF-1 and (right) IRMOF-16 (from the University of Liverpool's ChemTube3D website [20].) This figure shows the Monte Carlo boxes which are 2 × 2 × 2 crystallographic supercell representations.

2. Pore structures

The slit-shaped carbon pore walls have been modeled by a pair of parallel graphene layers. The size of the pores studied in this paper varied between 1nm and 2nm. The pore width has been defined as the distance between the centers of the carbon atoms in the graphene sheet. The CH_4–graphene interaction has been described by the standard analytical Steele potential [15–18]. This potential assumes that a CH_4 molecule interacts with carbon atoms in the graphene sheet through the Lennard–Jones (6–12) potential and renders the energy of the adsorbed particle as an integral over the whole graphene sheet. To account for the atomic structure of graphite, the energy can be modulated by adding a corrugation term. However, atomic corrugation of the graphitic wall is not explicitly treated in this paper as it represents a small fraction of the CH_4–wall interaction energy. Its influence is negligible for the total storage capacity [15,18].

IRMOFs [11] are three-dimensional cubic networks constructed from Zn_4O coordination centers connected by dicarboxylate linkers. Two such structures have been chosen here to study CH_4 adsorption, IRMOF-1 (also called MOF-5) and IRMOF-16. The linkers used in these structures are benzene-dicarboxylate and triphenyl-dicarboxylate linkers, respectively [11]. We used the crystallographic information files (.cif) for both IRMOFs from the Cambridge Crystallographic Data Centre (CCDC) website under codes CSD-175572

for IRMOF-1 and CSD-175585 for IRMOF-16 [11,19]. Table 1 summarizes some key features for both IRMOFs while Fig. 1 gives graphical representations of their unit cells. The unit cell dimensions of both systems are comparable; the most important difference between them is that IRMOF-16's unit cell contains one pore (cage) of a single type and IRMOF-1's unit cell contains 8 pores (cages) of two different types. Fig. 1 shows the 2 × 2 × 2 supercells, with the crystallographic unit cells doubled in each direction.

The IRMOF walls are strongly heterogeneous, both energetically and structurally. This characteristic is illustrated in Fig. 2, which shows the difference between the distributions of CH_4 energy, when methane is adsorbed in the 1nm carbon slit pore and in IRMOF-1.

Table 1: Key characteristics for IRMOF-1 and IRMOF-16 [11].

Structure	Unit cell dimensions Å	Simulation cell volume / Å^3	Free pore volume /%	Crystal density / g.cm
IRMOF-1	25.83200	17238	79.2	0.61
IRMOF-16	21.49030	9925	91.1	0.21

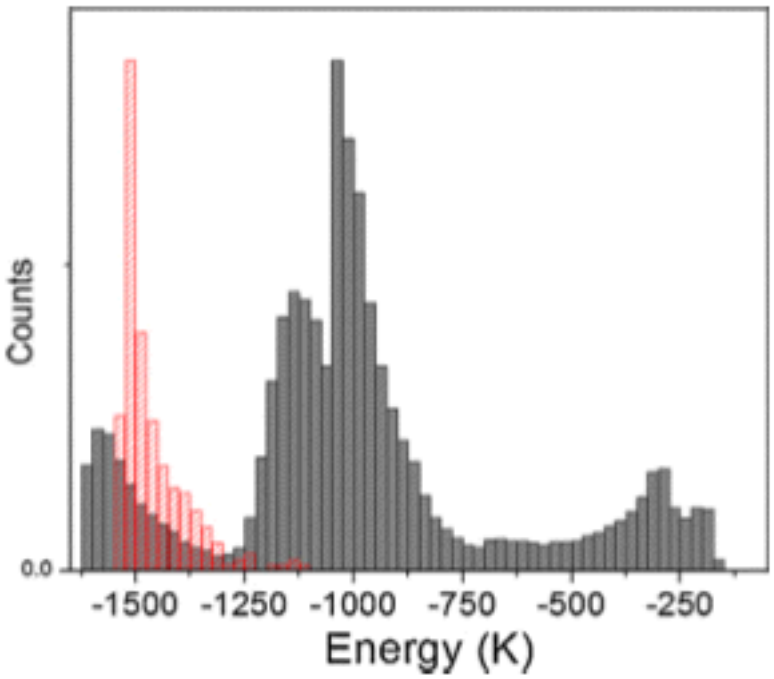

Fig. 2. Distributions of the interaction energy between CH4 molecules and the pore wall in 1 nm slit-shaped pore (red, shaded distribution) and in IRMOF-1 (gray, solid distribution). (For interpretation of the references to color in this figure legend, the reader is referred to the web version of this article.)

3. Simulation method

The computational approach was based on the GCMC simulations [21] implemented in the Music software package [22]. The MOF framework was considered rigid during simulations, meaning that its atoms were kept fixed at their crystallographic positions. All interatomic interactions were modeled using the Lennard–Jones (6–12) potential. The parameters for the framework atoms were obtained from the Universal Force Field (UFF) [23]. The CH_4 molecules were considered as super atoms (united atom model). The CH_4 –CH_4 Lennard–Jones parameters were $\sigma_{CH_4} = 3.730$ Å and $\varepsilon_{CH_4} = 148.0$ K [24]. Parameters describing fluid–solid interactions were obtained using the Lorentz–Berthelot mixing rules. The inter- actions were cut off beyond 12.8 Å [25]. Due to the symmetry of the super atom representation of the CH_4 molecules, electrostatic forces were not considered in the simulations. Periodic boundary conditions were employed in all directions.

All simulations were carried out at four temperatures: 80, 110, 140, and 180 K. Isotherm points were calculated by averaging the number of adsorbed molecules per unit cell of the material for a given chemical potential μ and temperature T. Each GCMC simulation was run for at least 60 million steps and consisted of insertion, deletion and displacement moves [22]. Thermodynamic properties for bulk CH_4 were calculated with NIST's REFPROP application [26].

4. Results

Fig. 3 shows the evolution of the CH_4 adsorption isotherms in both systems: carbon slit pores and IRMOFs at T = 80, 110, 140, and 180 K. The isotherms show the number of molecules adsorbed in the pores. The volumes of the slit pores are 4.26 × 4.92 × 1.0 nm^3 for the smaller slit pore and 4.26 × 4.92 × 2.0 nm^3 for the larger slit pore. The volumes of the MOFs' cells have been normalized to vol- umes having the same xy base surface. The IRMOF-1 base surface (1.291 × 1.291 nm^2) has been used to represent the isotherms in Fig. 3. The third dimension (z) has been defined by the pore sizes and was equal to 1.291 nm and 2.149 nm for IRMOF-1 and IRMOF-16, respectively.

Several differences between the CH_4 adsorption isotherms in both systems can be noted. First of all, the stepwise character of the isotherms, a characteristic of layer formation and observed in slit pores (Fig. 3, left panel), is modified in the IRMOF environ- ment (Fig. 3, right panel). Although the 1 nm slit pore and IRMOF-1 isotherms seem similar, the microscopic configurations of both structures are totally different. In the slit pore a regular mono- layer forms on each wall surface, whereas in IRMOF-1 the adsorbate structure evolution with pressure is much more complicated and shows a non-continuous reconstruction before the pores are filled up (see discussion below). The main factor responsible for these differences is the structure of the pore walls. At the temperatures studied here the graphene walls can be considered as homogeneous; their atomic corrugation has been neglected in the model of CH_4 pore wall interaction. At the same time, the IRMOF adsorbing walls are strongly heterogeneous within the crystallographic unit cell (Fig. 1) from both geometric and energetic points of view. The heterogeneity of the adsorption sites in IRMOFs is defined by the various atoms of the solid walls; the strongest adsorption sites are the metallic centers and the weaker ones are located on the organic linkers. Therefore we conclude that the similarity of adsorption isotherms in both systems is only apparent and is a consequence of the very small size of the IRMOF-1 pore which results in relatively strong energies of adsorption (Fig. 4). The mechanism of the layer formation is very different, as will be seen from the density evolution discussed below.

The influence of the adsorption sites' strong heterogeneity on the mechanism of adsorption is much more easily observed in larger pores. Methane adsorption in 2nm carbon slits gives rise to a stepwise isotherm; the resulting adsorbed structure consists of regular methane layers. In IRMOF-16 the stepwise adsorption is not observed at all. The first layer is formed in a very continuous way and over a relatively large range of pressure. It confirms that there is a distribution of adsorption energies in the system. At low temperatures (below 110 K), once the first layer covers the walls, the pore is rapidly filled up. At higher temperatures thermal fluctuations modify the mechanism of adsorption and all discontinuous changes disappear. This phenomenon is well known in nanopores where the critical points of transition depend on structural and energetic characteristics of the pore [14].

Analysis of the adsorption energies (Fig. 4) provides additional insight into the mechanism of adsorption. In slit pores, the absolute value of energy always increases when the first layer is formed. This is a consequence of the formation of ordered layers where absolute energy increases with the density of the layer. The average adsorption energy slightly decreases when the second layer is adsorbed in the 2nm pore. This decrease is a consequence of the smaller contribution of the adsorbate–adsorbent interactions, in particular for the second layer. The situation is different in IRMOFs. In IRMOF-1 the general trend is similar to the one observed in the 1 nm slit pore. However, due to the heterogeneous wall structure, the energy increase is more gradual. In IRMOF-16 the observed energy decrease is typical for heterogeneous surfaces. The filling of the pore is accompanied by a small discontinuous rise and then stabilization of the energy, indicating condensation of a liquid layer in the center of the pore. It is interesting to note that in both the 2 nm slit pore and IRMOF-16, the formation of the second layer shows many characteristics of capillary condensation. However, we do not want to call it capillary condensation because there is no way of form- ing a meniscus in the microporous

space. It is rather an analog of the layering transition observed in the slit pores. At the same time, there is no layer which is formed because of the 3D symmetry (cubic in the studied case) of the porous framework. So, we observe that the rapid adsorption (at 80 and 110 K) which fills up the pore is a consequence of relatively strong methane–methane interaction which stabilizes the systems. Its mechanism is more similar to the structural phase transformations than to capillary condensation or layering transition. At higher temperatures the filling is more grad- ual due to the thermal fluctuations but the average energy always increases.

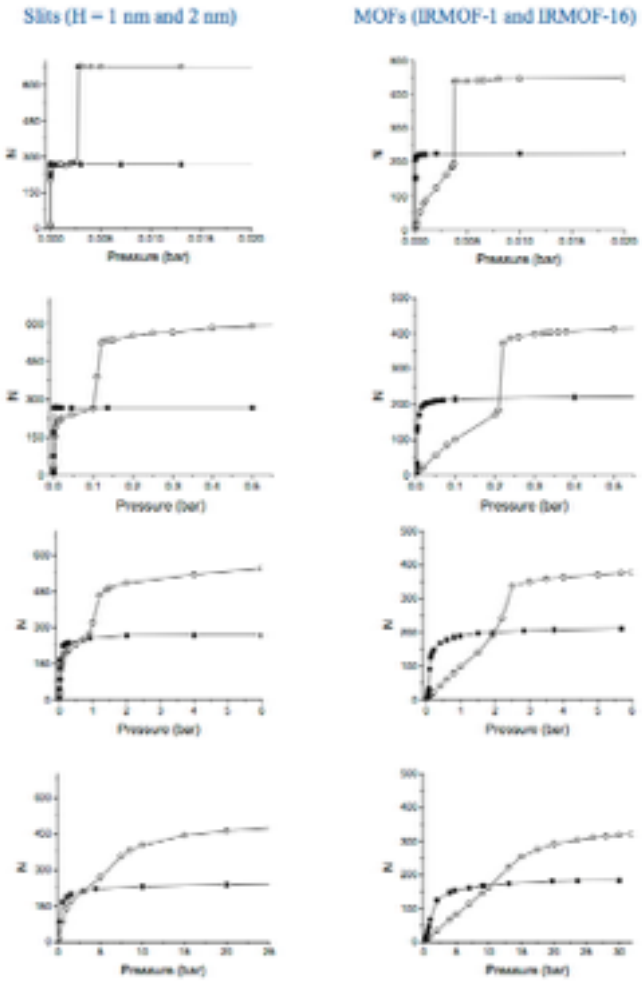

Fig. 3. Isotherms of CH_4 adsorption in (left): carbon slit pores with widths of 1.0 nm (full squares) and 2.0 nm (open circles), (right): IRMOF-1 (full squares) and IRMOF-16 (open circles). Temperatures from top to bottom are 80 K, 110 K, 140 K, and 180 K, respectively. N gives the number of methane molecules in a normalized volume having the same xy base surface (see text).

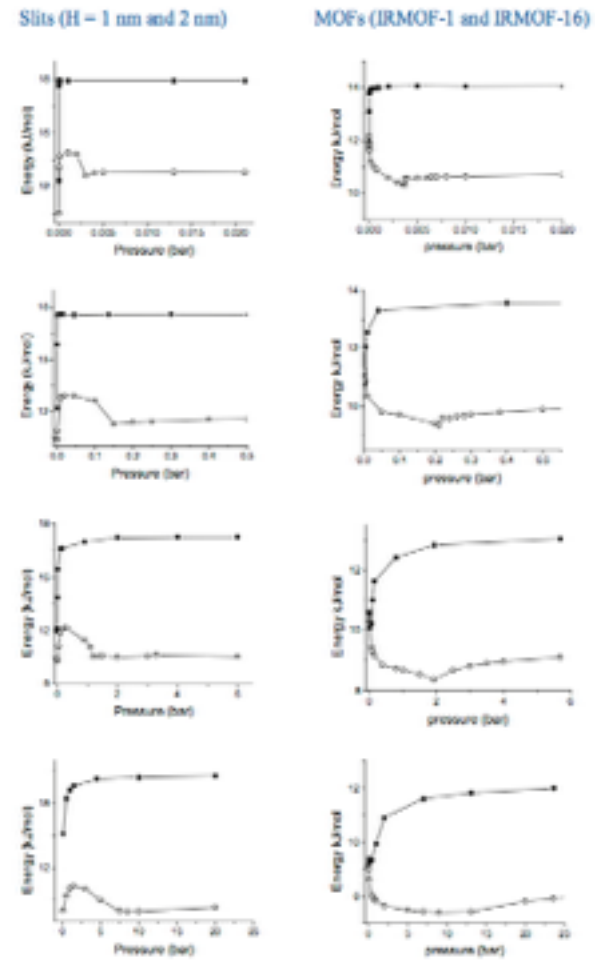

Fig. 4. Absolute values of CH_4 adsorption energies for (left): carbon slit pores with widths of 1.0 nm (full squares) and 2.0 nm (open circles), (right): IRMOF-1 (full squares) and IRMOF-16 (open circles). Temperatures from top to bottom are 80 K, 110 K, 140 K, and 180 K, respectively.

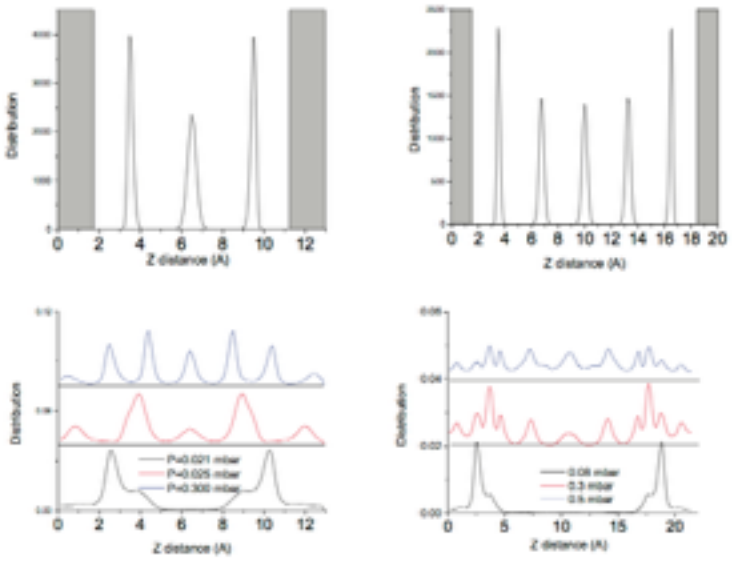

Fig.5.Cumulative density distribution of methane adsorbed at 80K. Top: adsorption in saturated slit pores (left:1.3 nm pore, right: 2 nm pore). The grey rectangles indicate the dead volume in the pore, due to the pore walls thickness. Bottom: the pressure dependence of the methane densities in IRMOF-1 (left) and IRMOF-16 (right). Pressure increases from the bottom to the top distribution.

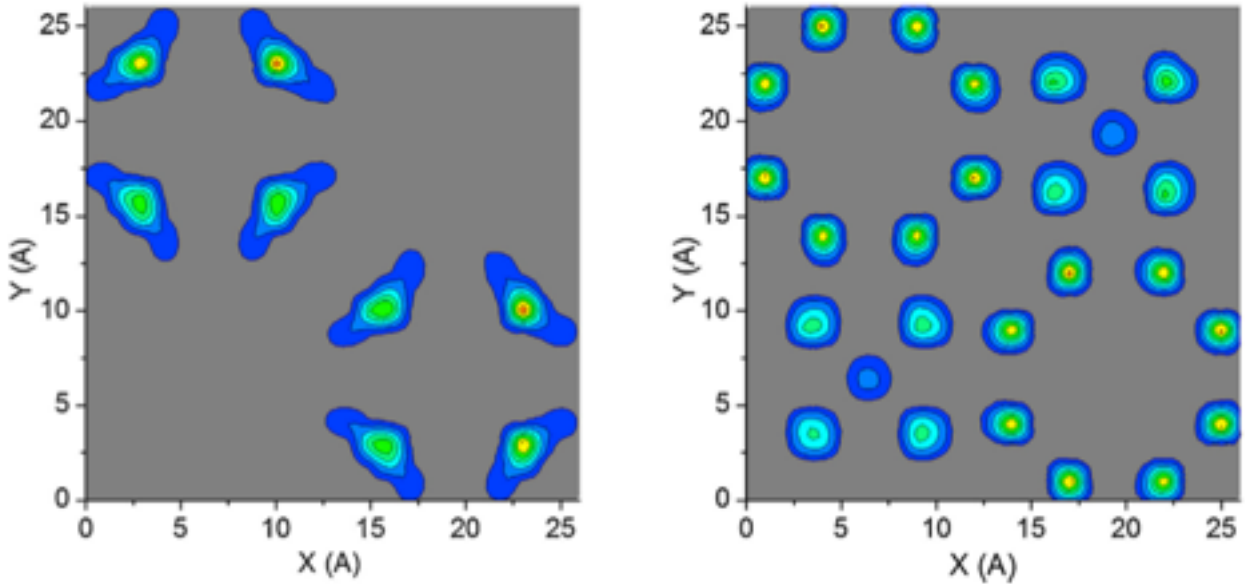

Fig. 6. Maps (xy plane) of density of methane adsorbed at 80 K in IRMOF-1: at 0.021 mbar (left) and at 0.025 mbar (right).

The trends observed for the isotherms and energies have their source in the allowed methane microscopic configurations. Fig. 5 shows the cumulative density distribution of methane adsorbed in slit-shaped pores and in IRMOFs. As expected, the density in the slit pores does not show any qualitative evolution as a function of pressure. It forms well defined layers where the positions of the peaks remain unchanged. The situation is more dynamic in IRMOF pores where the positions of the peaks are pressure dependent. It means that the 3D order of adsorbate is adjusting itself to the quantity of adsorbed gas and they can change very rapidly with small pressure variation. A close analysis of the peak positions clearly indicates that the distribution of adsorbed molecules (density) undergoes structural transformations: its low and high pressure orders are very different, especially in the IRMOF-1 structure. Not only does the number of peaks change but their positions are also changing in a non-continuous way.

Fig. 6 shows the spectacular transformation of the methane density distributions between 0.021 mbar and 0.025 mbar in IRMOF-1. In spite of a very small pressure variation, the adsorbate under- goes a discontinuous qualitative reconstruction. With increasing pressure, the symmetry of the methane structure changes. This transformation seems to indicate an evolution, as a function of pressure, of the distribution of accessible adsorption sites in the heterogeneous MOF structure. The transformation shows characteristics of a conventional structural phase transition.

The observed layering adsorption mechanism in the slit pores is coherent with the previous simulation by Miyahara and Gubbins [27,28]. There are no structural changes which would lead to structures with different symmetry. Only solid–liquid transformations are possible within each layer. The observed transitions at 80 K in IRMOF-1 structure are much more intricate. Below 0.023 mbar there is already adsorbed methane which occupies less than 15% of the total capacity. The transformations above 0.023 mbar could be interpreted as formation of two contact layers (~0.75 of the total capacity) followed by formation of the middle layer above 0.027 mbar, as it happens in the 1.3 nm slit pore (see the slit pore distribution in Fig. 5). However, in the MOF structure each step leads to a profound reconstruction of the lower pressure structure. It is visualized by the mass distributions (Fig. 5) and even better by the xy maps of the mass distribution shown in Fig. 6. The latter one proves that part of the volume which was already filled at lower pressure is rebuilt and another part of the unit cell is filled in. The detailed mechanism of this transition requires more fundamental studies.

5. Conclusions

We have compared the mechanism of adsorption of methane in two types of microporous structures: carbon slit-shaped pores with homogeneous pore walls and heterogeneous MOF-type structures.

Methane adsorption progresses through typical layer-by-layer filling of the pores. This mechanism of layering transition, clearly observed in the slit pores [27,28], is strongly modified in the MOFs with strongly heterogeneous walls where formation of the first layer is more gradual. At the same time, in MOFs, the adsorbate structure undergoes important density redistribution as a function of pressure. This feature is not observed in slit pores where the density distribution (the position of the maxima) is pressure- independent.

The microscopic mechanism of methane adsorption in IRMOF- 1 is discontinuous. At low temperature (<140 K) methane fills the pore through a discrete number of states. These states are characterized by different distributions of methane density, as shown in Figs. 5 and 6. The adsorption of the first layer in IRMOF-16 is continuous and shows typical characteristics of heterogeneous surfaces. The formation of the second layer shows characteristics of capillary condensation: when the pore is filled in, the condensate inside the pore is more strongly bonded than the monolayer structure. At higher temperatures (140 K and 180 K) the adsorption mechanism shows continuous filling of pores in both IRMOF-1 and IRMOF-16 systems.

Summing up, the mechanism of pore filling in IRMOF-1 and IRMOF-16 is complex and involves an important structural reconstruction of the adsorbed phase at 80 K and 110 K. This trans- formation is induced by an evolution of the preferred adsorption sites as a function of gas pressure. It shows some features characteristic of structural phase transitions in the 3D (bulk) systems: in particular, a modification of the adsorbate structure symmetry is observed. This transition occurs due to the ordered but strongly heterogeneous distribution of adsorption sites in MOFs and is not observed in structurally homogeneous slit pores. Comparing the slit and the MOF wall geometry, on can say that the structural changes of adsorbate in MOF are analogs of the layering transitions in the slit pores. However, due to the very heterogeneous walls, they lead to profound reconstruction of the already adsorbed structure.

Acknowledgment

ED would like to thank the PACA Region for financial support under the Exploratory Call; grant ‘PACE’ no. 2013 04267.

References

[1] J.P. Marco-Lozar, M. Kunowsky, J.D. Carruthers, A. Linares-Solano, Gas storage scale-up at room temperature on high density carbon materials, Carbon 76 (2014) 123–132.
[2] S. Ma, H.-C. Zhou, Gas storage in porous metal-organic frameworks for clean energy applications, Chem. Commun. 46 (2010) 44–53.
[3] W. Wang, D. Yuan, Mesoporous carbon originated from non-permanent porous MOFs for gas storage and CO2/CH4 separation, Sci. Rep. 4 (2014) 1–7.
[4] A.R. Millward, O.M. Yaghi, Metal-organic frameworks with exceptionally high capacity for storage of carbon dioxide at room temperature, J. Am. Chem. Soc. 127 (2005) 17998–17999.
[5] M.B. Sweatman, N. Quirke, Characterization of porous materials by gas adsorption at ambient temperatures and high pressure, J. Phys. Chem. B 105 (2001) 1403–1411.
[6] P. Benard, R. Chahine, Storage of hydrogen by physisorption on carbon and nanostructured materials, Scr. Mater. 56 (2007) 803–808.
[7] F. Rouquerol, J. Rouquerol, K. Sing, P. Llewellyn, G. Maurin, Adsorption by Powders and Porous Solids, Principles, Methodology and Applications, second ed., Academic Press, Oxford, 2014.
[8] S. Cavenati, C.A. Grande, A.E. Rodrigues, Adsorption equilibrium of methane, carbon dioxide, and nitrogen on zeolite 13× at high pressures, J. Chem. Eng. Data 49 (2004) 1095–1101.
[9] J. Rowsell, A. Millward, K. Park, O.M. Yaghi, Hydrogen sorption in functionalized metal-organic frameworks, J. Am. Chem. Soc. 126 (2004) 5666–5667.
[10] N.L. Rosi, J. Eckert, M. Eddaoudi, D.T. Vodak, J. Kim, M. O’Keeffe, O.M. Yaghi, Hydrogen storage in microporous metal–organic frameworks, Science 300 (2003) 1127–1129.
[11] M. Eddaoudi, J. Kim, N.L. Rosi, D.T. Vodak, J. Wachter, M. O’Keeffe, O.M. Yaghi, Systematic design of pore size and functionality in isoreticular mofs and their application in methane storage, Science 295 (2002) 469–472.
[12] D. Fairen-Jimenez, N.A. Seaton, T. Düren, Unusual adsorption behavior on metal–organic frameworks, Langmuir 26 (2010) 14694–14699.
[13] K.S. Walton, A.R. Millward, D. Dubbeldam, H. Frost, J.J. Low, O.M. Yaghi, R.Q. Snurr, Understanding inflections and steps in carbon dioxide adsorption isotherms in metal–organic frameworks, J. Am. Chem. Soc. 130 (2007) 406–407.
[14] M. De Toni, P. Pullumbi, F.-X. Coudert, A.H. Fuchs, Understanding the effect of confinement on the liquid–gas transition: a study of adsorption isotherms in a family of metal–organic frameworks, J. Phys. Chem. C 114 (2010) 21631–21637.

[15] B. Kuchta, L. Firlej, A. Mohammadhosseini, P. Boulet, M. Beckner, J. Romanos, P. Pfeifer, Hypothetical high-surface-area carbons with exceptional hydrogen storage capacities: open carbon frameworks, J. Am. Chem. Soc. 134 (2012) 15130–15137.
[16] B. Kuchta, L. Firlej, P. Pfeifer, C. Wexler, Numerical estimation of physical limits of hydrogen storage by physisorption in microporous nanospaces, Carbon 48 (2010) 223–231.
[17] L. Firlej, S. Roszak, B. Kuchta, P. Pfeifer, C. Wexler, Enhanced hydrogen adsorption in boron substituted carbon nanospaces, J. Chem. Phys. 131 (2009) 164702.
[18] R.D. Etters, B. Kuchta, J. Belak, Vacancy-induced melting of N2 adlayers on graphite, Phys. Rev. Lett. 70 (1993) 826–829.
[19] F.H. Allen, The Cambridge Structural Database: a quarter of a million crystal structures and rising, Acta Crystallogr. Sect. B: Struct. Crystallogr. Cryst. Chem. B 58 (2002) 380–388.
[20] N. Greeves, http://www.chemtube3d.com/solidstate/MOF-home.html 2008–2014.
[21] D. Frenkel, B. Smit, Understanding Molecular Simulations from Algorithms to Applications, second ed, Academic Press, San Diego, 2002.
[22] A. Gupta, S. Chempatha, M.J. Sanborna, L.A. Clark, R.Q. Snurr, Object-oriented programming paradigms for molecular modeling, Mol. Simul. 29 (2003) 29–46.
[23] A.K. Rappe, C.J. Casewit, K.S. Colwell, W.A. Goddard III, W.M. Skiff, UFF, a full periodic table force field for molecular mechanics and molecular dynamics simulations, J. Am. Chem. Soc 114 (1992) 10024–10035.
[24] S.J. Goodbody, K. Watanabe, D. MacGowan, J.P.R.B. Walton, N. Quirke, Molecular simulation of methane and butane in silicalite, J. Chem. Soc. Faraday Trans. 87 (1991) 1951.
[25] T. Dü ren, L. Sarkisov, O.M. Yaghi, R.Q. Snurr, Design of new materials for methane storage, Langmuir 20 (2004) 2683–2689.
[26] E.W. Lemmon, M.L. Huber, M.O. McLinden, NIST standard reference database 23: reference fluid thermodynamic and transport properties-REFPROP, version 9.1, Natl. Inst. Stand. Technol., Stand. Ref. Data Progr. Gaithersburg (2013).
[27] M. Miyahara, K.E. Gubbins, Freezing/melting phenomena for Lennard–Jones methane in slit pores: a Monte Carlo study, J. Chem. Phys. 106 (1997) 2865.
[28] S. Jiang, C.L. Rhykerd, K.E. Gubbins, Layering, freezing transitions, capillary condensation and diffusion of methane in slit carbon pores, Mol. Phys. 79 (1993) 373–391, 1993.